

# Efficient photocatalyst based on ZnO nanorod arrays/*p*-type boron-doped-diamond heterojunction

Shiyong Gao · Shujie Jiao · Bin Lei ·  
Hongtao Li · Jinzhong Wang · Qingjiang Yu ·  
Dongbo Wang · Fengyun Guo · Liancheng Zhao

Received: 10 October 2014 / Accepted: 8 November 2014 / Published online: 25 November 2014  
© Springer Science+Business Media New York 2014

**Abstract** The ZnO nanorod arrays (NRs) have been fabricated on *p*-type boron-doped diamond (BDD) substrate by hydrothermal method. It was demonstrated that the density and diameter of the ZnO NRs can be effectively controlled by adjusting the reactant concentration. Photocatalytic activity of the fabricated ZnO NRs/*p*-BDD heterojunction was investigated for the degradation of methyl orange dye and the results indicated that diameter and density of ZnO NRs play a very important role in photocatalytic degradation. Furthermore, the ZnO NRs/*p*-BDD heterostructure photocatalysts are easily recycled and reused.

## 1 Introduction

In recent years, considerable efforts have been made to hunt for a low-cost and effective method in order to solve growing water pollution problem which is serious harmful to the human health [1]. Semiconductor photocatalysis, as a “green” method, has been used to mineralize organic pollutants into harmless carbon dioxide, water and other inorganic compounds without bringing secondary pollution,

showing a good application prospect. Titanium dioxide (TiO<sub>2</sub>), with bandgap of 3.2 eV, is one of the most researched semiconductor oxides in photocatalytics for degradation of organic pollutants [2]. ZnO, a direct bandgap *n*-type semiconductor, having similar bandgap (3.37 eV) and band edge positions as TiO<sub>2</sub> [3], was attracted tremendous interest as a candidate in photocatalytics. Especially compared with TiO<sub>2</sub>, ZnO exhibits higher electron mobility and longer electron lifetime [4]. Furthermore, ZnO could be fabricated into diverse morphologies with much better feature using different methods [5–7]. Therefore, ZnO is a promising alternative for the degradation of organic pollutants. However, a major limit of low quantum yield hinders ZnO as a photocatalyst in practical application, which is normally caused by the rapid recombination of photogenerated electron–hole pairs [8]. In order to overcome the disadvantage, various methods have been developed to reduce the recombination rate of photogenerated electrons and holes. Among these methods, semiconductor-based heterostructure has received much attention recently because it can provide a potential driving force to achieve efficient charge separation and faster carrier migration [9].

Various types of heterostructured photocatalysts, such as ZnO–CdS, ZnO–ZnS and ZnO–Bi<sub>4</sub>Ti<sub>3</sub>O<sub>12</sub> have been widely investigated [10–12]. However, the recollection and reuse of those photocatalysts still limit the practical application [13]. Supported photocatalysts that can be easily separated is a feasible way for large-scale photocatalysis applications [14]. Diamond has many super properties such as highest thermal conductivity, hardness, good chemical and temperature stabilities, could be used as an ideal substrate for the immobilization of photocatalysts [15, 16]. More importantly, the conduction band (CB) of ZnO is positioned between the CB and valence band (VB) of diamond, and the VB of ZnO is positioned below the VB of

---

S. Gao · S. Jiao (✉) · B. Lei · H. Li · J. Wang · Q. Yu (✉) ·  
D. Wang · F. Guo · L. Zhao  
School of Materials Science and Engineering, Harbin Institute  
of Technology, Harbin 150001, China  
e-mail: shujiejiao@gmail.com

Q. Yu  
e-mail: qingjiang.yu@hit.edu.cn

S. Jiao  
Key Laboratory for Photonic and Electric Bandgap Materials,  
Ministry of Education, Harbin Normal University,  
Harbin 150001, China

diamond. When boron-doped diamond (BDD) combined with ZnO, a type II junction was formed at the interface, which could hinder the charge recombination and improve the photocatalytic efficiency.

In this paper, ZnO nanorod arrays (NRs) on BDD film were successfully synthesized by hydrothermal method. The *n*-type ZnO NRs/*p*-type BDD heterojunctions which have been achieved show highly efficient photocatalytic activities. The effects of diameter and density of ZnO NRs on the photocatalytic properties of ZnO NRs/*p*-type BDD heterojunction were discussed.

## 2 Experimental section

### 2.1 Sample preparation

The ZnO NRs on BDD were prepared by hydrothermal method similar to our previous report [17]. Typically, aqueous solution of zinc acetate dihydrate ( $\text{Zn}(\text{CH}_3\text{COOH})_2 \cdot 2\text{H}_2\text{O}$ ) and hexamethylenetetramine (HMT,  $(\text{CH}_2)_6\text{N}_4$ ) aqueous solution of equal concentration (0.01, 0.025, 0.05 and 0.1 mol/L) were mixed under mild magnetic stirring for 10 min. Then the solution was transferred into the Teflon-lined stainless steel autoclave with a volume of 50 mL. The BDD films coated with ZnO seed layer were vertically immersed into the solution. Subsequently, the autoclave was heated to a constant temperature of 95 °C for 24 h. Finally, the autoclave was cooled down naturally. The obtained samples were thoroughly washed with distilled water to remove the residual salts and dried naturally in air.

### 2.2 Characterization

The morphology, chemical composition, and crystal structure of the as-fabricated samples were characterized by means of scanning electron microscope (SEM, PHIL-IPSEXL-3) with energy dispersive X-ray spectrometry (EDS) and X-ray diffraction (XRD, Bruke D8 advance with Cu K $\alpha$  radiation). Raman spectra were measured by a Renishaw inVia Raman microscope with an argon ion laser ( $\lambda$ , 514 nm). The electrical properties of BDD films were obtained by the van der Pauw method at room temperature in a HALL8800 system.

### 2.3 Photocatalytic activity measurements

The photocatalytic activities of the as-synthesized products were evaluated using methyl orange (MO), a typical pollutant in textile industry, as a model organic contaminant in water. The obtained product used with an area of 1 cm<sup>2</sup> was vertically immersed in the 10 mg/L MO solution filled in a quartz tube, and irradiated by a 500 W xenon lamp

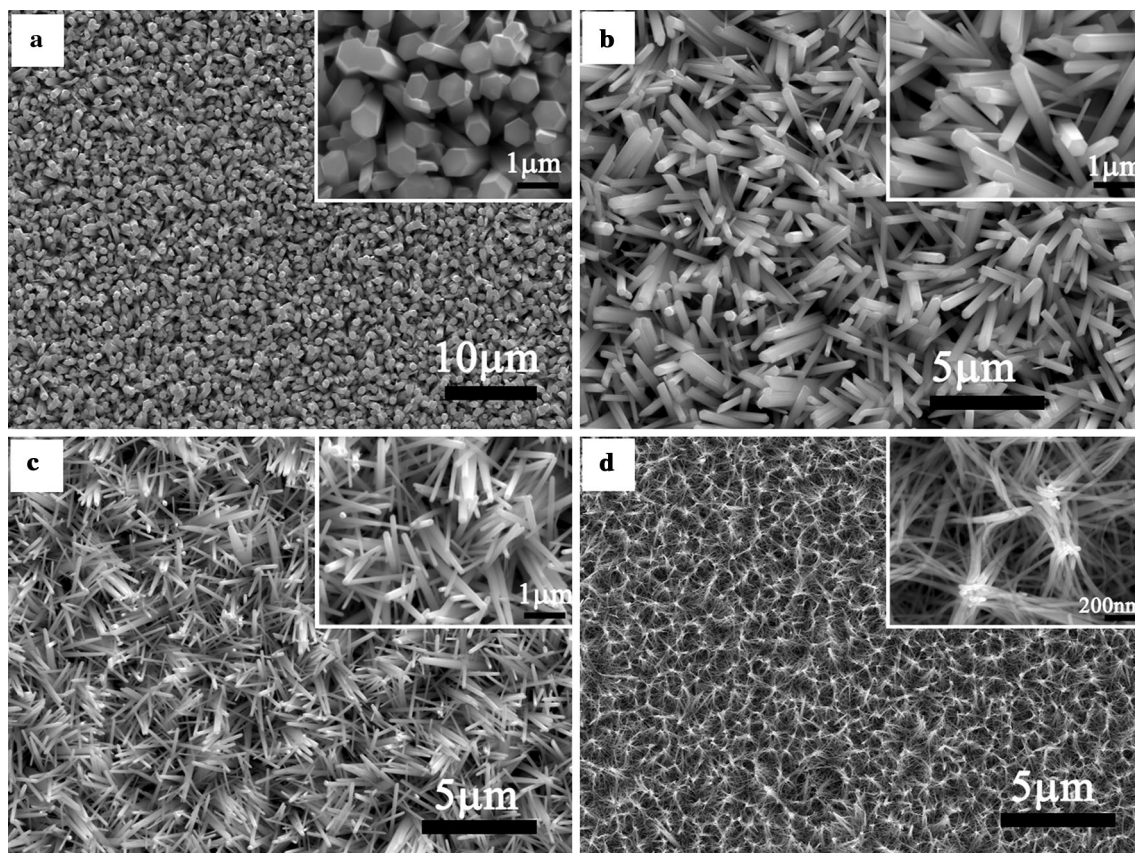
(CEL-S500). After a given irradiation time, the MO concentration was evaluated by UV–visible spectrophotometer (Phenix, UV1700PC) monitoring the absorption maximum at  $\lambda_{\text{max}} = 465$  nm.

## 3 Results and discussion

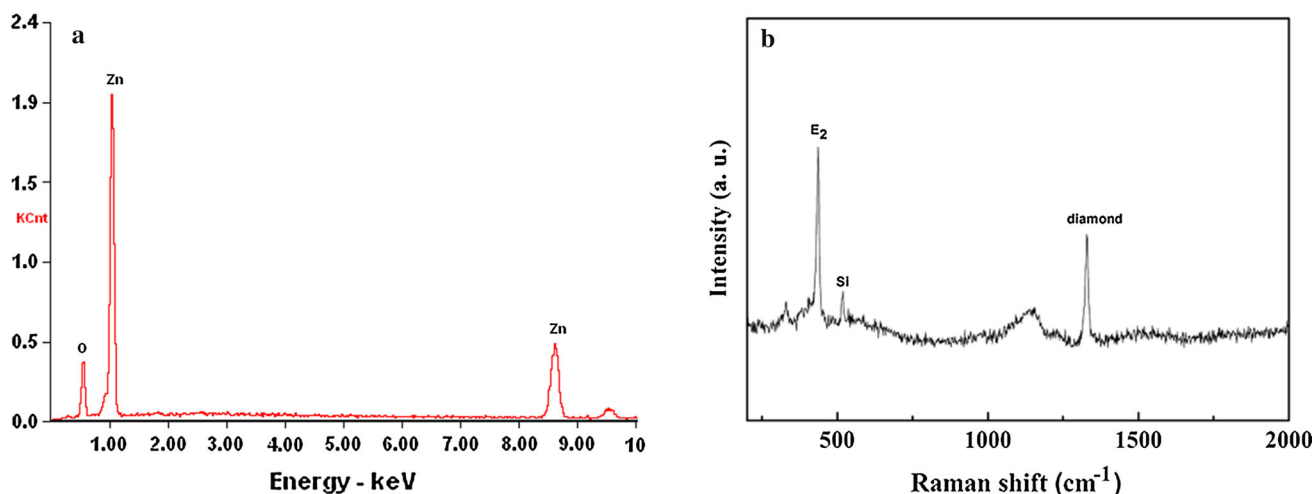
The BDD films showed *p*-type conduction with a hole concentration of  $7.3 \times 10^{19}$  cm<sup>-3</sup> at room temperature. After the hydrothermal reaction, very thin homogenous films were coated on the surface of BDD substrates. Figure 1 shows typical morphologies of the as-prepared products grown at different concentrations of the aqueous solution containing equimolar concentrations of  $\text{Zn}(\text{CH}_3\text{COOH})_2 \cdot 2\text{H}_2\text{O}$  and HMT. A large amount of ZnO NRs for all samples were uniformly distributed on the entire surface of the substrate. When the reactant concentration was 0.1 mol/L, the ZnO nanorods exhibited the smooth regular hexagonal top facets with an average diameter of about 600 nm and bonded tightly together (shown in Fig. 1a). As the concentration was decreased to 0.05 mol/L, Fig. 1b shows decrease in the diameter of ZnO nanorods and increase in the space between the nanorods. When the reactant concentration was decreased to 0.025 mol/L, the diameter of ZnO nanorods decreases continuously to 100 nm while obvious change is found for nanorod density in Fig. 1c. With the further decrease of reactant concentration to 0.01 mol/L, the ZnO nanorods with diameter of 20 nm were formed, and the array density continued to increase (shown in Fig. 1d). Since ZnO nanorods are too thin to be individually stood, they became to be inclined and intertwined with each other and a reticular structure forms, herein that the gap distance between NRs was increased.

Figure 2a, b show the EDS and Raman spectrum of synthesized ZnO NRs with reactant concentration of 0.025 mol/L. The EDS spectrum (Fig. 2a) shows that only the Zn and O elements are present in the sample, confirming a high purity of the as prepared ZnO NRs. In Raman spectrum (Fig. 2b), a sharp peak at around 1330 cm<sup>-1</sup> dominates the spectrum, which is asymmetry and downshift with respect to the intrinsic zone-centre phonon band of diamond at 1332 cm<sup>-1</sup> due to Fano interference [18]. The peaks at 332 and 437 cm<sup>-1</sup> are assigned to the 3E<sub>2H</sub>–E<sub>2L</sub> and E<sub>2</sub> (high) mode of ZnO [19], respectively. In addition, the sharp peak at 519 cm<sup>-1</sup> is the phonon mode originated from Si substrate.

Figure 3 shows the XRD patterns of ZnO NRs deposited on the BDD substrates with different reactant concentrations. Evidently, all the diffraction peaks present in each sample, besides the peaks assigned to diamond (111) planes, can be indexed as wurtzite-structured (hexagonal)



**Fig. 1** SEM images and high-magnification images (*the inset*) of the synthesized ZnO NRs with different reactant concentration: **a** 0.1, **b** 0.05, **c** 0.025, and **d** 0.01 mol/L



**Fig. 2** **a** The EDS spectrum and **b** Raman spectrum of synthesized ZnO NRs with reactant concentrations of 0.025 mol/L

ZnO. The narrow diffraction peaks indicate that the ZnO NRs are highly crystallized. Moreover, the intensities of the diffraction peaks of ZnO increase with increase of the reactant concentration demonstrating an increased quantity of obtained ZnO products.

To evaluate the photocatalytic activities of the ZnO NRs/*p*-BDD heterojunction, samples were carried out to test the degradation efficiency in decomposing MO solution, as shown in Fig. 4a. The degradation efficiency is defined as  $C/C_0$ , where  $C$  is the concentration of MO

solution at the irradiation time  $t$ ,  $C_0$  is the initial concentration. The blank experiment (without photocatalyst) showed that a very slight increase in the MO concentration due to evaporation of the solution, indicating that the photoinduced self-decomposition may be neglected. From Fig. 4a, it can be clearly seen that the degradation efficiency was greatly accelerated with the addition of ZnO NRs/ $p$ -BDD. With decreasing of the reactant concentration from 0.1 to 0.025 mol/L, the photocatalytic activity of the ZnO NRs/ $p$ -BDD heterojunction increases. However, a further decrease in reactant concentration leads to a reduction of the photocatalytic activity. It indicates that the reactant concentration for as-synthesis of ZnO NRs/ $p$ -BDD

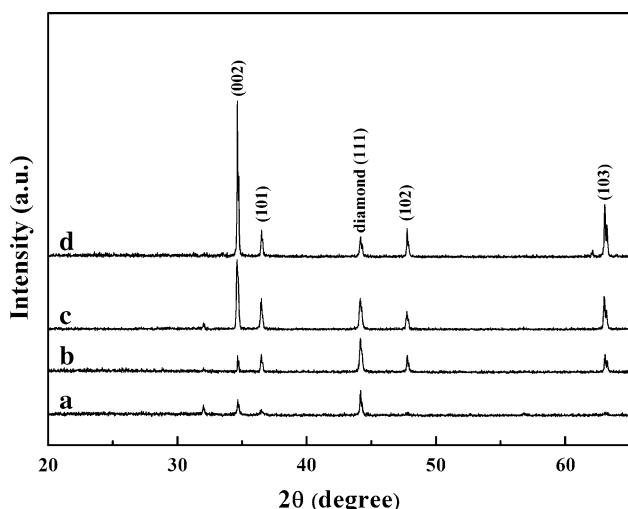


**Fig. 3** XRD patterns of the ZnO samples grown on BDD films with different reactant concentrations: (a) 0.01, (b) 0.025, (c) 0.05, and (d) 0.1 mol/L

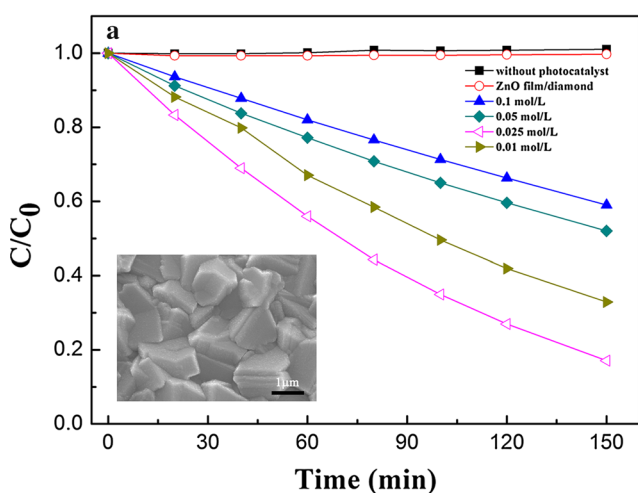


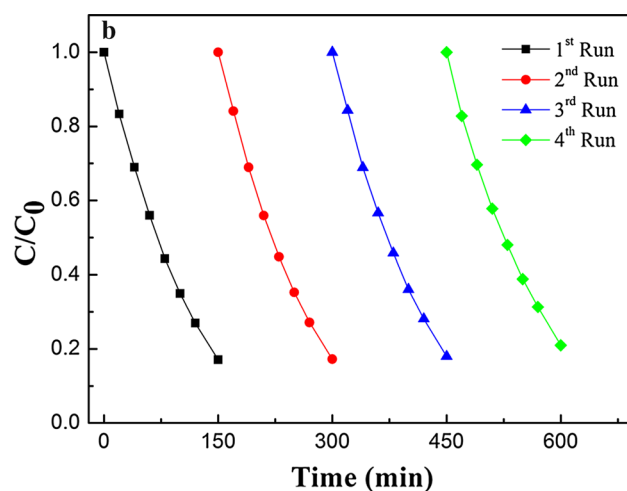
**Fig. 4 a** The photocatalytic MO degradation efficiency of ZnO NRs/ $p$ -BDD heterojunction prepared at different reactant concentration, ZnO film/ $p$ -BDD heterojunction, and without photocatalyst for reference. The inset is the SEM image of the ZnO film deposited

heterojunction take significant effects on the photocatalytic activity and the sample obtained with the reactant concentration of 0.025 mol/L has the highest photocatalytic activity.

The stability of the ZnO NRs/ $p$ -BDD photocatalyst was also evaluated. Figure 4b shows that there is only slightly loss in the degradation efficiency after four cycles, which indicates that the ZnO NRs/BDD heterojunction have good stability and reusability.

Based on the experimental results, the mechanism of the photocatalytic activity of the ZnO NRs/ $p$ -diamond heterojunction has been proposed. There are two control factors influencing MO photocatalytic degradation. As shown in Fig. 5, ZnO and BDD can form a type-II heterojunction. When the ZnO NRs/ $p$ -BDD heterostructure is illuminated by UV light from the ZnO side, electrons ( $e^-$ ) in the VB can be excited to the CB leaving the same amount of holes ( $h^+$ ) in the VB. Subsequently, the photogenerated electrons (holes) transfer from the CB of  $p$ -diamond (VB of ZnO) to the CB of ZnO (VB of  $p$ -diamond) under electric field located at the interface between ZnO and BDD, and the probability of the recombination of electron-hole pairs are significantly reduced. Consequently, the highly efficient electron- and hole-related redox processes would occur for the degradation [20].

On the other hand, the diameter and density of ZnO NRs, and open space between neighboring nanorods have influences on the photocatalytic activity as well. The ZnO NRs with high density and small diameter could enhance the surface-to-volume ratio, which provides sufficient exposed positions for the easy absorption of UV light. Meanwhile, the UV light could reach the BDD side surface through space



on BDD substrate. **b** Recyclability test of photocatalytic decomposition for synthesized ZnO NRs/ $p$ -BDD heterojunction with reactant concentrations of 0.025 mol/L

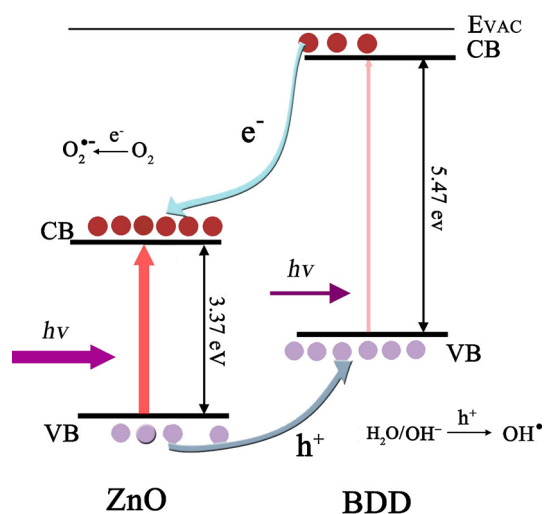


**Fig. 5** Schematic band diagram of ZnO NRs/*p*-diamond heterojunction and the transfer processes of photogenerated carriers

between neighboring nanorods and the BDD could generate photogenerated electron–hole pairs, which could enhance the photoactivity [16]. More importantly, a wide separation between neighboring nanorods will allow easy diffusion of MO into the inner region of the arrays and arrive at exposed BDD surface for photocatalytic reaction. Therefore, as the decrease in diameter and increase in density of ZnO NRs, the photocatalytic activity is greatly enhanced.

In order to verify our results, about 2  $\mu\text{m}$ -thickness ZnO thin films were deposited on BDD films by radio frequency. From Fig. 4a, it can be clearly seen that the ZnO film/*p*-BDD heterojunction displays very poor photocatalytic activity. Thus, it is illustrated that the heterojunction of ZnO thin film and BDD play a weak role in photocatalytic degradation of MO in this case due to the limited MO and UV light arriving at BDD surface, because the entire BDD surface was fully covered with the continuous ZnO film (the inset of Fig. 4a). However, a further decrease in diameter and increase in density of ZnO NRs, the amount of the obtained ZnO products (photocatalyst) obviously decreased, which will result in a significant decrease in photocatalytic activity. It is believed that a proper diameter and density of ZnO NRs play a very important role in photocatalytic degradation.

#### 4 Conclusions

In summary, ZnO NRs were successfully grown on the BDD substrate by the simple hydrothermal method. According to experimental results, the density and diameter of ZnO NRs can be controlled by adjusting the reactant concentration. It is found that the photocatalytic activity of ZnO NRs/*p*-BDD heterojunction depends on the diameter,

density of ZnO NRs, the space between the nanorods and heterojunction structure in the interface between ZnO and BDD. Furthermore, the ZnO NRs/*p*-BDD heterostructure photocatalysts are easily recycled and reused. Considering the unique excellent properties of ZnO and diamond, we expect that the ZnO NRs/*p*-BDD will offer promising application in the field of wastewater treatment.

**Acknowledgments** The work was financially supported by National Science Foundation (No. 61306014), the Research Fund for the Doctoral Program of Higher Education of China (No. 20122302120009), the China Postdoctoral Science Foundation (No. 2013M540283), Heilongjiang Province Postdoctoral Science Foundation (No. LBH-Z11142), the Fundamental Research Funds for the Central Universities (No. HIT. NSRIF. 2014003), Harbin Special Fund for Creative Talents in Science and Technology (No. 2012RFLXG029), and Open Project Program of Key Laboratory for Photonic and Electric Bandgap Materials, Ministry of Education, Harbin Normal University (No. PEBM201302).

#### References

- J.L. Zhang, Y.M. Wu, M.Y. Xing, S.A.K. Leghari, S. Sajjad, *Energy Environ. Sci.* **3**, 715–726 (2010)
- S.L. Xie, X.H. Lu, T. Zhai, J.Y. Gan, W. Li, M. Xu, M.H. Yu, Y.M. Zhang, Y.X. Tong, *Langmuir* **28**, 10558–10564 (2012)
- I. Gonzalez-Valls, M. Lira-Cantu, *Energy Environ. Sci.* **2**, 19–34 (2009)
- M. Quintana, T. Edvinsson, A. Hagfeldt, G. Boschloo, *J. Phys. Chem. C* **111**, 1035–1041 (2007)
- S.J. Sun, S.J. Jiao, K.J. Zhang, D.B. Wang, H.T. Li, S.Y. Gao, J.Z. Wang, Q.J. Yu, F.Y. Guo, L.C. Zhao, S.C. Su, *J. Mater. Sci. Mater. Electron.* **24**, 85–88 (2013)
- H.B. Lu, B.H. Dong, L. Zhao, S.M. Wang, Z.X. Xu, J.C. Li, *J. Mater. Sci. Mater. Electron.* **23**, 1905–1909 (2012)
- Z.L. Wang, *Mater. Today* **7**, 26–33 (2004)
- H. Tong, S.X. Ouyang, Y.P. Bi, N. Umezawa, M. Oshikiri, J.H. Ye, *Adv. Mater.* **24**, 229–251 (2012)
- H.G. Kim, P.H. Borse, W.Y. Choi, J.S. Lee, *Angew. Chem. Int. Ed.* **44**, 4585–4589 (2005)
- J. Ouyang, M. Chang, X. Li, *J. Mater. Sci.* **47**, 4187–4193 (2012)
- H.X. Sang, X.T. Wang, C.C. Fan, F. Wang, *Int. J. Hydrog. Energy* **37**, 1348–1355 (2012)
- X.B. Meng, J. Miao, Y. Zhao, S.Z. Wu, X.G. Xu, S.G. Wang, Y. Jiang, *J. Mater. Sci. Mater. Electron.* **25**, 1423–1428 (2014)
- H.M. Zhu, B.F. Yang, J. Xu, Z.P. Fu, M.W. Wen, T. Guo, S.Q. Fu, J. Zuo, S.Y. Zhang, *Appl. Catal. B: Environ.* **90**, 463–469 (2009)
- F.F. Brites, V.S. Santana, N.R.C. Fernandes-Machado, *Top. Catal.* **54**, 264–269 (2011)
- J.M. Liu, Y.B. Xia, L.J. Wang, Q.F. Su, W.M. Shi, *J. Cryst. Growth* **300**, 353–357 (2007)
- J.J. Yuan, H.D. Li, S.Y. Gao, Y.H. Lin, H.Y. Li, *Chem. Commun.* **46**, 3119–3121 (2010)
- S.Y. Gao, D.M. Li, Y.A. Li, X.Y. Lv, J.Z. Wang, H.T. Li, Q.J. Yu, F.Y. Guo, L.C. Zhao, *J. Alloys Compd.* **539**, 200–204 (2012)
- Y.G. Wang, S.P. Lau, B.K. Tay, X.H. Zhang, *J. Appl. Phys.* **92**, 7253–7256 (2002)
- S.J. Chen, Y.C. Liu, Y.M. Lu, J.Y. Zhang, D.Z. Shen, X.W. Fan, *J. Cryst. Growth* **289**, 55–58 (2006)
- Q. Yu, J. Li, H.D. Li, Q.L. Wang, S.H. Cheng, L.A. Li, *Chem. Phys. Lett.* **539–540**, 74–78 (2012)